Potential Energy Surfaces of the Gas-Phase S_N2 Reactions $X^- + CH_3X = XCH_3 + X^-$ (X = F, Cl, Br, I): A Comparative Study by Density Functional Theory and ab Initio Methods

Liqun Deng, Vicenç Branchadell,† and Tom Ziegler*

Contribution from the Department of Chemistry, University of Calgary, Calgary, Alberta, Canada T2N 1N4

Received April 8, 1994®

Abstract: We have explored the potential energy surfaces of the title reactions by density functional theory (DFT) and ab initio methods. The DFT calculations were based on the local density approximation (LDA) as well as the more sophisticated approach, NL-SCF, in which nonlocal corrections are included self consistently. The ab initio methods made use of the Hartree−Fock (HF) scheme as well as up to fourth-order Møller−Plesset perturbation theory (MP4). We have systematically characterized the geometries, frequencies, and energies for the reactants, ion−dipole complexes, and the transition states. Our study shows that the DFT methods offer overall better geometries and frequencies than the HF and MP2 schemes in comparison with the experimental results. In predicting the C−X bond energies of the reactants, CH_3X, the NL-SCF scheme is superior to all other methods applied in this study. The NL-SCF and MP4 complexation energies are similar and in good agreement with the experimental results for all but the fluorine system, for which the NL-SCF value is about 6 kcal/mol larger than the MP4 estimate. For the transition state energies, i.e., the barrier heights, the ab initio and DFT results turn out to be qualitatively different in the order HF ≫ MP2 > MP4 ≫ NL-SCF ≫ LDA. The experimental data seem to fall into the region with the MP4 and NL-SCF values as the upper and lower bounds, respectively. Within the DFT approaches, the relativistic effects on the geometries, frequencies, and energies were discussed, and the intrinsic reaction coordinate (IRC) method was utilized to provide further information about the potential energy surfaces, and to rationalize the reaction mechanism. We finally carried out bond energy decomposition and population analyses on the X−C bonds formed or broken during the reaction processes studied here.

I. Introduction

The bimolecular exchange reaction between methyl halides and halogen anions

$$X^- + CH_3X = XCH_3 + X^-; \quad X = F, Cl, Br, \text{and } I \qquad (1)$$

has served over the past years as the prototype for S_N2 substitution reactions.[1] It has in addition been used extensively as a model in studies involving molecular dynamics,[2] chemical kinetics,[3] isotope[4] and solvation[5] effects, and gas-phase photochemistry.[6] A common theme in all of these studies has been the characterization of the potential energy surface along the reaction path for (1). Early theoretical[7] and experimental[7e] gas-phase studies have established an energy profile for (1) of the form given in Figure 1. The profile has a double well shape with two minima symmetrically situated around a central energy barrier. The two minima represents identical ion−dipole complexes between CH_3X and X^-, and the barrier corresponds to the transition state. The profile in Figure 1 can thus be characterized by the stability of the ion−dipole complex, ΔE_0^C, and the barrier height, ΔE_0^B, or the intrinsic barrier, E_0^{IB}, as defined in the following equations:

$$\Delta E_0^C = E_0(X^-\cdots CH_3X) - E_0(X^- + CH_3X) \qquad (2)$$

$$\Delta E_0^B = E_0([X\cdots CH_3\cdots X]^-) - E_0(X^- + CH_3X) \qquad (3)$$

$$\Delta E_0^{IB} = E_0([X\cdots CH_3\cdots X]^-) - E_0(X^-\cdots CH_3X) \qquad (4)$$

It is difficult to extract conclusive information about the profile of (1) from experiments.[3b,8] Thus, quantum chemical calculations provide the only source for a detailed characterization of the potential energy surface along the reaction path. However, theoretical ab initio calculations on reaction paths are demanding since an accurate account of electron correlation is required. It is thus necessary to go beyond the simple Hartree−Fock (HF) approach. The first ab initio calculation beyond HF

† Permanent address: Department de Química, Universitat Autònoma de Barcelona, 08193 Bellaterra, Spain.

® Abstract published in *Advance ACS Abstracts*, October 1, 1994.

(1) Shaik, S. S.; Schlegel, H. B.; Wolfe, S. *Theoretical Aspects of Physical Organic Chemistry. The S_N2 Mechanism*; Wiley: New York, 1992.

(2) Cho, Y. J.; Vande Linde, S. R.; Zhu, L.; Hase, W. L. *J. Chem. Phys.* **1992**, *96*, 8275 and references therein.

(3) (a) Barlow, S. E.; Van Doren, J. M.; Bierbaum, V. M. *J. Am. Chem. Soc.* **1988**, *110*, 7240. (b) Mekel, A.; Havlas, Z.; Zahradnik, R. *J. Am. Chem. Soc.* **1988**, *110*, 8355. (c) Tucker, S. C.; Truhlar, D. G. *J. Am. Chem. Soc.* **1990**, *112*, 3339.

(4) (a) Wolfe, S.; Kim, C. K. *J. Am. Chem. Soc.* **1991**, *113*, 8056. (b) Boyd, R. J.; Kim, C. K.; Shi, Z.; Weinberg, N.; Wolfe, S. *J. Am. Chem. Soc.* **1993**, *115*, 10147. (c) Poirier, R. A.; Wang, Y.; Westaway, K. C. *J. Am. Chem. Soc.* **1994**, *116*, 2526.

(5) (a) Certner, B. J.; Whitnell, R. M.; Wilson, K. R.; Hynes, J. T. *J. Am. Chem. Soc.* **1991**, *113*, 74. (b) Tucker, S. C.; Truhlar, D. G. *J. Am. Chem. Soc.* **1990**, *112*, 3347.

(6) (a) Cyr, D. M.; Scarton, M. G.; Johnson, M. A. *J. Chem. Phys.* **1993**, *99*, 4869. (b) Cyr, D. M.; Bishea, G. A.; Johnson, M. A. *J. Chem. Phys.* **1992**, *97*, 5911.

(7) (a) Dedieu, A.; Veillard, A. *J. Am. Chem. Soc.* **1972**, *94*, 6730. (b) Dedieu, A.; Veillard, A. In *Quantum Theory of Chemical Reactions*; Daudel, R., Pullman, A., Salem, L., Veillard, A., Eds.; Reidel: Dordrecht, 1979, and references therein. (c) Wolfe, S.; Mitchell, D. J.; Schlegel, H. B. *J. Am. Chem. Soc.* **1981**, *103*, 7692. (d) Wolfe, S.; Mitchell, D. J.; Schlegel, H. B. *J. Am. Chem. Soc.* **1981**, *103*, 7694. (e) Pellerite, M. J.; Brauman, J. I. *J. Am. Chem. Soc.* **1983**, *105*, 2672 and references therein.

(8) (a) DePuy, C. H.; Gronert, S.; Mullin, A.; Bierbaum, V. M. *J. Am. Chem. Soc.* **1990**, *112*, 8650. (b) Brauman, J. I.; Olmstead, W. N.; Lieder, C. A. *J. Am. Chem. Soc.* **1974**, *96*, 4030.

0002-7863/94/1516-10645$04.50/0

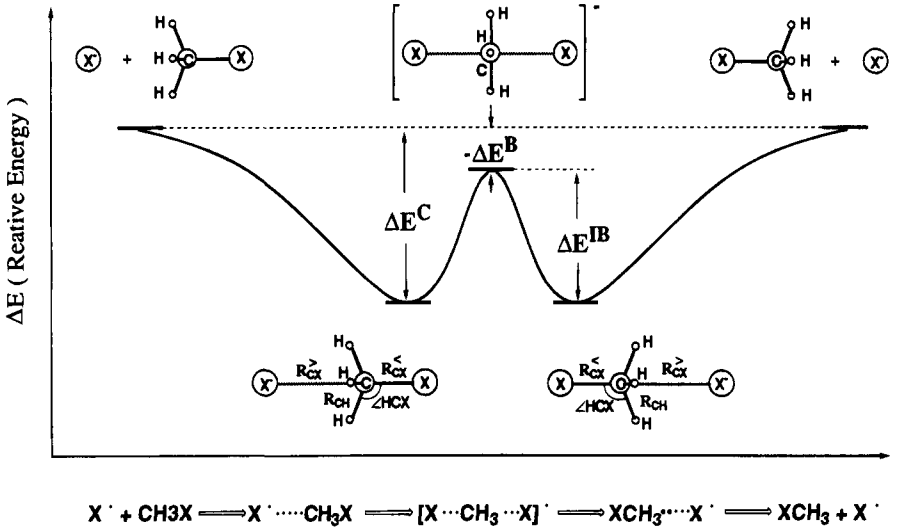

Figure 1. An illustration of the potential energy surface and reaction mechanism for the gas-phase S_N2 reactions: $X^- + CH_3X = [X\cdots CH_3\cdots X]^- = CH_3X + X^-$ (X = F, Cl, Br, I).

on the gas-phase S_N2 reactions was carried out by Dedieu and Veillard.[7a] Since then, several post-HF ab initio calculations have been reported.[9] High-level ab initio calculations on (1) for X = F and Cl are now available.[10] For $Br^- + CH_3Br$ only one limited post-HF calculation has been reported so far,[10d] and for $I^- + CH_3I$ no sophisticated ab initio results are available for the transition state structure and barrier.[10g]

Density functional theory[11] (DFT) has recently emerged as an alternative to traditional ab initio methods in studies on molecular energetics and kinetics.[12] We shall in this investigation apply DFT to reaction 1 for the entire family of halogens X = F, Cl, Br, and I. Our study will provide optimized geometrical structures, calculated harmonic vibrational frequencies, and relative energies for the reactants (products), $X^- + CH_3X$, ion–dipole complexes, $X^-\cdots CH_3$, and transition states, $[X\cdots CH_3\cdots X]^-$. The intrinsic reaction pathways (IRP's) will also be presented for the chlorine system. We have previously shown that DFT results provide as good a fit to experiment as high-level ab initio findings in studies on elementary reaction steps involving organic molecules.[12]

It is the purpose of the present study to compare results from DFT and high-level ab initio calculations on the profile of (1). We have, in order to carry out such a comparison, applied DFT to (1) for all halogens. Calculations based on Møller–Plesset perturbation theory to fourth order (MP4) were in addition carried out for X = Br and I, since systematically high-level post-HF ab initio studies are lacking for these reactions systems. With the aim of assessing basis set and correlation effects on the relative energies, we have also carried out calculations on the fluorine system with the most extensive basis set, TZ3P+R+(2f,d),[10a] at the HF and MP2 level. We hope further through estimates of ΔE^C and ΔE^B to provide reliable reaction profiles that might be used as input in dynamic gas-phase calculations, derivation of rate constants from statistical methods, as well as the simulation of solvation effects based on molecular dynamics or Monte Carlo techniques.

II. Computational Methods

The ab initio calculations reported in this study were carried out by using the GAUSSIAN 92 program package.[13] For X = Br and I the geometry optimization and frequency calculations were performed at the MP2 level. Additional single point energy calculations based on the MP2 optimized geometries were carried out at the full MP4SDTQ level. The basis set used in these calculations was of 6-31G(d,p) quality for C and H, while for Br and I, use was made of the compact effective potentials (CEP) due to Stevens et al.[14] augmented by a d-polarization function as well as a set of diffuse s and p functions (CEP-31++G-(d)). For the fluorine system, the MP2(full)/6-31++(p,d) optimized geometries due to Shi and Boyd[10b] were used for single point energy calculations at the HF and MP2(full) levels with the most extensive basis set, TZ3P+R+(2f,d) (F,C(11s7p3d2f/6s5p3d2f) and H(6s3p1d/4s3p1d)),[10a] and the MP4-MP2 corrections[10a] were estimated by use of the standard 6-311++G(d,p) basis set.

The ADF program system developed by Baerends et al.[15] was used for all DFT calculations. The geometries and corresponding energies were calculated at two levels of theory. At the lower level use was made of the local density approximation (LDA)[16] with the parametrization due to Vosko et al.[17] At the higher level LDA was augmented by inclusion of Perdew's[18] gradient based correlation correction and Becke's[19] nonlocal exchange correction in the SCF procedure (NL-SCF).[20] For comparison, the single point energies based on the LDA geometries were also estimated by introducing the nonlocal corrections into the LDA energies as a perturbation based on the LDA density (NL-P). The relativistic effects on the geometries, energetics, and

(9) (a) Keil, F.; Ahlrichs, R. *J. Am. Chem. Soc.* **1976**, *98*, 4787. (b) Urban, M.; Čemuša'k, I.; Kellö, V. *Chem. Phys. Lett.* **1984**, *105*, 625. (c) Serre, J. *Int. J. Quantum Chem.* **1984**, *26*, 593. (d) Cernusak, I.; Urban, M. *Collect. Czech. Chem. Commun.* **1988**, *53*, 2239.

(10) (a) Wladkowski, B. D.; Lim, K. F.; Allen, W. D.; Brauman, J. I. *J. Am. Chem. Soc.* **1992**, *114*, 9136 and references therein. (b) Shi, Z.; Boyd, R. J. *J. Am. Chem. Soc.* **1990**, *112*, 6789. (c) Shi, Z.; Boyd, R. J. *J. Am. Chem. Soc.* **1989**, *111*, 1575. (d) Vetter, R.; Zülicke, L. *J. Am. Chem. Soc.* **1990**, *112*, 5136. (e) Tucker, C. S.; Truhlar, D. G. *J. Phys. Chem.* **1989**, *93*, 8138. (f) Shi, Z.; Boyd, R. J. *J. Am. Chem. Soc.* **1991**, *113*, 2423. (g) Hu, W.; Truhlar, D. G. *J. Phys. Chem.* **1994**, *98*, 1049.

(11) (a) Ziegler, T. *Chem. Rev.* **1991**, *91*, 651. (b) *Density Functional Methods in Chemistry*, Labanowski, J., Andzelm, J., Eds.; Springer-Verlag: New York, 1991. (c) Parr, R. G.; Yang, W. *Density-Functional Theory of Atoms and Molecules*; Oxford University Press: New York, 1989.

(12) (a) Deng, L.; Ziegler, T. *Int. J. Quantum Chem.* **1994**, *52*, 731. (b) Deng, L.; Ziegler, T.; Fan, L. *J. Chem. Phys.* **1993**, *99*, 3823. (c) Fan, L.; Ziegler, T. *J. Am. Chem. Soc.* **1992**, *114*, 10890. (d) Fan, L.; Ziegler, T. *J. Chem. Phys.* **1990**, *92*, 3645.

(13) Gaussian 92, Frisch, M. J.; Trucks, G. W.; Head-Gordon, M.; Gill, P. M. W.; Wong, M. W.; Foresman, J. B.; Johnson, B. G.; Schlegel, H. B.; Robb, M. A.; Replogle, E. S.; Gomperts, R.; Andres, J. L.; Raghavachari, K.; Binkley, J. S.; Gonzalez, C.; Martin, R. L.; Fox, D. J.; DeFrees, D. J.; Baker, J.; Stewart, J. J. P.; Pople, J. A. Gaussian, Inc., Pittsburgh, PA, 1992.

(14) Stevens, W. J.; Krauss, M.; Basch, H. *Can. J. Chem.* **1992**, *70*, 612.

(15) Baerends, E. J.; Ellis, D. E.; Ros, P. *Chem. Phys.* **1973**, *2*, 41.

(16) Gunnarson, O.; Lundquist, I. *Phys. Rev.* **1974**, *B10*, 1319.

(17) Vosko, S. H.; Wilk, L.; Nusair, M. *Can. J. Phys.* **1980**, *58*, 1200.

(18) Perdew, J. P. *Phys. Rev.* **1986**, *B33*, 8822. Erratum: *Ibid.* **1986**, *B34*, 7406.

(19) Becke, A. D. *Phys. Rev.* **1988**, *A38*, 3098.

(20) Fan, L.; Ziegler, T. *J. Chem. Phys.* **1991**, *94*, 6057.

Table 1. Geometrical Parameters for Methyl Halides, CH_3X (X = F, Cl, Br, I)[a]

	R_{CX}				R_{CH}				∠HCX			
halogen (X)	LDA[b]	NL-SCF[b]	MP2[c,d]	expt[e]	LDA[b]	NL-SCF[b]	MP2[c,d]	expt[e]	LDA[b]	NL-SCF[b]	MP2[c,d]	expt[e]
F	1.375	1.400	1.406	1.382	1.100	1.099	1.090	1.095	109.3	108.7	108.1	108.5
Cl	1.754	1.778	1.779	1.785	1.096	1.095	1.089	1.090	109.2	108.2	108.9	108.1
Br	1.930	1.967	1.949	1.933	1.094	1.094	1.083	1.086	108.3	107.5	107.9	107.7
I	2.115	2.156	2.150	2.132	1.094	1.093	1.083	1.084	108.3	107.3	107.7	107.7

[a] See Figure 1 for a definition of geometrical parameters; distances in angstroms, and angles in degrees. [b] This work, TZ+2P basis set. [c] X = F and Cl ref 10b with 6-31++G(d,p) basis set. [d] X = Br and I, this work, CEP-31++G(d) basis for Br and I, and 6-31G(d,p) basis set for C and H. [e] Reference 28.

frequencies for the bromine and iodine systems were evaluated by the quasirelativistic (QR) method.[21]

An uncontracted triple-ζ STO basis set[22] plus two 3d STO polarization functions were adapted for the carbon and halogen atoms. For the hydrogen atom, the triple-ζ basis augmented by three 2p STO functions was used. The frozen-core approximation[15] was applied to all non-hydrogen atoms with *ns*, *np* as the valence shell. A set of auxiliary[23] s, p, d, f, and g STO functions, centered on all nuclei, was used to fit the molecular density and to present Coulomb and exchange-correlation potentials accurately in each SCF cycle.

The numerical integration procedure applied in the calculations was developed by te Velde et al.[24] The geometry optimization procedure was based on the analytical gradient method developed by Versluis and Ziegler.[25a] Vibrational frequencies were evaluated at the LDA level from force constants calculated by numerical differentiation of the energy gradients.[25b] The transition state structures were optimized by using the geometry optimization procedure under certain symmetry constraints.

The bond energy (ΔE_{BE}) decompsition scheme used to analyze the C−X bonds within the DFT framework was performed by an extended transition state (ETS) method due to Ziegler and Rauk.[26] The ETS method writes the bond energy as

$$\Delta E_{BE} = -(\Delta E_{elst} + \Delta E_{Pauli} + \Delta E_{orbit} + \Delta E_{prep}) \qquad (5)$$

The first term in (5) is the electrostatic interaction energy between two fragments from which the bond is formed. The second component arises from the Pauli exchange repulsion, due to the interaction between fully occupied spin orbitals on the two fragments of the same spin polarization. The sum of ΔE_{elst} and ΔE_{Pauli} is customarily referred to as steric interaction energy, ΔE_{steric}. The third term of eq 5 is due to the orbital interaction between occupied and empty spin orbitals on the two fragments of the same spin. This term can be further partitioned according to symmetry.[26] The last term, the perparation energy, represents the energy required to relax the geometry from a free fragment to that of the fragment in the molecular skeleton. All ETS calculations were executed at the NL-P//SCF-NL level.

The intrinsic reaction pathways were traced by the intrinsic reaction coordinate (IRC) method due to Fukui[27a] in an algorithm developed by Gonzalez and Schlegel[27b] and incorporated into the DFT-based schemes by Deng and Ziegler.[12a,b]

III. Results and Discussion

This section contains detailed analyses of the stationary points along the reaction path for the gas-phase S_N2 process (1). The analysis involves calculations on the geometric structures, vibrational frequencies, X−CH_3 bond strengths, relative energies of the stationary points, and the intrinsic reaction pathways. A comparison will also be carried out between results based on the DFT schemes and ab initio methods. Results from the same level of theory are finally used to establish trends within the halogen family.

A. Reactants. We start our discussion with the reactants. Experimental data for the gas-phase methyl halides are well established in terms of geometrical parameters, vibrational frequencies, and X−CH_3 bond strengths. It is thus possible to evaluate the accuracy of the different methods used here by applying them to calculations on the properties mentioned above.

Table 1 summarizes the geometrical parameters of the reactants determined by the LDA and NL-SCF schemes as well as the MP2 method. The most recent experimental data[28] are also listed in Table 1 for comparison. It follows from Table 1 that the three levels of theory provide reasonable fits to the experimental geometries. The root-mean-square (rms) absolute error for the eight bond lengths in Table 1 is 0.014, 0.017, and 0.012 Å for LDA, NL-SCF, and MP2 results, respectively. For bond angles the NL-SCF data compare more favorable with the experimental results than the LDA and MP2 values. The data compiled in Table 1 reflect a general tendency of the MP2[29] and DFT[29a,30] methods. Relativistic effects[21b,31] were found to have a negligible influence on the structures of the molecules studied here with a slight elongation of the C−I bond by 0.005 Å. We shall in the following sections base all geometry optimizations on nonrelativistic calculations.

Table 2 compares frequencies based on MP2 and LDA calculations with experimental values for the reactants CH_3X. It can be deduced from Table 2 that the average deviations of the LDA results from the experimentally observed fundamental frequencies[32] are 2.0, 3.5, 2.6 and 2.6% for CH_3F, CH_3Cl, CH_3Br, and CH_3I, respectively. These values should be compared with the corresponding discrepancies due to MP2 of 5.1, 6.8, 6.1, and 6.4%, respectively. A comparison of the theoretical results with experimental harmonic frequencies[33] reveals the familiar trend[11a] where the LDA frequencies generally are too low, whereas the MP2 values systematically are too high. The average error of all the theoretical values in Table 2 relative to the experimentally harmonic frequencies is 3.6% for the LDA

(21) (a) Ziegler, T.; Tschinke, V.; Baerends, E. J.; Snijders, J. G.; Ravenek, W. *J. Phys. Chem.* **1989**, *93*, 3050 and references therein. (b) Schreckenbach, G.; Ziegler, T.; Li, J. *Int. J. Quantum Chem.* Submitted for publication.

(22) (a) Snijders, J. G.; Baerends, E. J.; Vernooijs, P. *At. Nucl. Data. Tables* **1982**, *26*, 483. (b) Vernooijs, P.; Snijders, J. G.; Baerends, E. J. *Slater Type Basis Functions for the Whole Periodic System*; Internal report; Free University of Amsterdam, The Netherlands, 1981.

(23) Krijn, J.; Baerends, E. J. *Fit functions in the HFS-method*; Internal Report (in Dutch); Free University of Amsterdam, The Netherlands, 1984.

(24) (a) Boerrigter, P. M.; te Velde, G.; Baerends, E. J. *Int. J. Quantum Chem.* **1988**, *33*, 87. (b) te Velde, G.; Baerends, E. J. *J. Comput. Phys.* **1992**, *99*, 84.

(25) (a) Versluis, L.; Ziegler, T. *J. Chem. Phys.* **1988**, *88*, 322. (b) Fan, L.; Versluis, L.; Ziegler, T.; Baerends, J. A.; Ravenek, W. *Int. J. Quantum Chem.* **1988**, *S22*, 173.

(26) (a) Ziegler, T.; Rauk, A. *Inorg. Chem.* **1979**, *18*, 1558. (b) Ziegler, T.; Rauk, A. *Inorg. Chem.* **1979**, *18*, 1755. (c) Ziegler, T.; Rauk, A. *Theor. Chim. Acta* **1977**, *46*, 1.

(27) (a) Fukui, K. *Int. J. Quantum Chem. Symp.* **1981**, *15*, 633. (b) Gonzalez, C.; Schlegel, H. B. *J. Phys. Chem.* **1990**, *94*, 5523.

(28) *CRC Handbook of Chemistry and Physics*, 74th ed.; Lide, P. R., Ed.; CRC Press: Boca Raton, FL, 1993.

(29) (a) Johnson, B. G.; Gill, P. M. W.; Pople, J. A. *J. Chem. Phys.* **1993**, *98*, 5612. (b) Hehre, W. J.; Radom, L.; Schleyer, P. v. R.; Pople, J. A. In *Ab Initio Molecular Orbital Theory*; Wiley-Interscience: New York, 1986.

(30) Dickson, R. M.; Becke, A. D. *J. Chem. Phys.* **1993**, *99*, 3898.

(31) Pyykkö, P. *Chem. Rev.* **1988**, *88*, 563.

(32) Schneider, W.; Thiel, W. *J. Chem. Phys.* **1987**, *86*, 923.

(33) (a) Duncan, J. L.; McKean, D. C.; Speirs, G. K. *Mol. Phys.* **1972**, *24*, 553. (b) Duncan, J. L.; Allan, A.; McKean, D. C. *Mol. Phys.* **1970**, *18*, 289.

Table 2. Vibrational Frequencies (cm^{-1}) for the Methyl Halides, CH_3X (X = F, Cl, Br, I)

vibrational modes	F				Cl				Br				I			
			expt				expt				expt				expt	
	LDA[a]	MP2[b]	fund[c]	harm[d]	LDA[a]	MP2[e]	fund[c]	harm[d]	LDA[a]	MP2[b]	fund[c]	harm[d]	LDA[a]	MP2[b]	fund[c]	harm[d]
$\omega_1(a_1)$	1087	1060	1049	1059	773	788	733	740	633	629	611	616	556	548	533	539
$\omega_2(e)$	1135	1228	1183	1206	976	1082	1018	1038	931	1010	955	934	865	943	882	900
$\omega_3(a_1)$	1415	1544	1459	1490	1308	1464	1355	1382	1282	1398	1305	1333	1225	1353	1251	1276
$\omega_4(e)$	1421	1566	1467	1498	1405	1545	1488	1481	1400	1532	1443	1472	1397	1526	1435	1464
$\omega_5(a_1)$	2946	3106	2920	3031	2996	3171	2968	3074	3039	3179	2958	3082	3011	3182	2955	3080
$\omega_6(e)$	3035	3219	2999	3131	3096	3289	3044	3166	3152	3306	3056	3184	3128	3309	3060	3188

[a] This work, TZ+2P basis set. [b] This work, 6-31(d,p) basis set for F, C, and H; CEP-31++G(d) basis set for Br and I. [c] Reference 32. [d] Reference 33. [e] Reference 10e, 6-31(d,p) basis set.

Table 3. $X-CH_3$ Bond Strength (kcal/mol) (X = F, Cl, Br, I)

halogen (X)	D_o°						ΔZVE		ΔE_{SO}	D_o°						
	LDA[a]	NL-P[a]	NL-SCF[a]	HF[b]	MP2[b]	MP4[b]	LDA[a]	MP2[b]	expt[c]	LDA[a]	NL-P[a]	NL-SCF[a]	HF[b]	MP2[b]	MP4[b]	expt[d]
F	144.5	118.2	118.3	67.2	111.0	107.0	−5.7	−6.0	−0.4	138.4	112.1	112.2	59.8	104.6	100.6	111.3
Cl	107.1	86.2	86.5	53.0	84.5	82.0	−4.8	−5.4	−0.8	101.5	80.6	80.9	46.8	78.3	75.8	81.9
Br	93.9	74.4	74.7	42.4	73.2	70.9	−4.6	−4.9	−3.5	85.8	66.3	66.6	34.0	64.8	62.5	68.6
I	82.5	63.9	64.5	33.0	62.6	60.8	−4.1	−4.5	−7.2	71.2	52.6	53.2	21.3	50.9	49.1	55.7

[a] This work, TZ+2P basis set; ΔZPE calculated from eq 9 by LDA frequencies. [b] This work, all *ab initio* results based on the MP2 geometries (see the text), 6-311G(d,p) basis set for H, C, F, and Cl; and CEP-31++G(d) basis set for Br and I; ΔZPE calculated from eq 9 by MP2 frequencies. [c] Reference 36. [d] Experimental D_o° values estimated from ΔH_0^{298} according to eq 10, also see footnote 38; and the experimental ΔH_0^{298} values taken from ref 28.

data and 3.7% for the MP2 results. We conclude that the LDA frequencies are comparable in quality to those obtained by the MP2 scheme.[10e]

The $X-CH_3$ bond strength is another crucial quantity related to (1). Table 3 compares bond energies determined by the different levels of theory with experimental[28,34] estimates. The $X-CH_3$ bond energies were estimated from the reaction enthalpy of the bond dissociation process:

$$CH_3X \rightarrow {}^\bullet CH_3 + X^\bullet; \qquad X = F, Cl, Br, \text{and } I \tag{6}$$

The electronic reaction enthalpy, D_e^0, of (6) at 0 K is given by:

$$D_e^\circ = E(X^\bullet) + E({}^\bullet CH_3) - E(CH_3X) \tag{7}$$

and the bond dissociation enthalpy, D_0°, at 0 K is then evaluated from the following equation:

$$D_o^\circ = \Delta H_0^\circ = D_e^\circ + \Delta ZPE + \Delta E_r \tag{8}$$

where ΔZPE is the vibrational zero point energy correction estimated by:

$$\Delta ZPE = \frac{hc}{2}[{}_i\sum \omega_i({}^\bullet CH_3) - {}_i\sum \omega_i(CH_3X)] \tag{9}$$

Here c is the speed of light, h is Plank's constant, and the sum is over the vibrational frequencies, ω_i. The term ΔE_r in eq 8 is the relativistic correction to the bond dissociation energy. It can be[21a] written as

$$\Delta E_r = \Delta E_{MD} + \Delta E_{SO} \tag{10}$$

Here ΔE_{MD} is the contribution to the bond energy from the scalar[21a] mass velocity and Darwin terms, whereas ΔE_{SO} represents the contribution from the spin−orbit coupling.[21a] The contribution from ΔE_{MD} is modest. It was calculated to be 0.1 kcal/mol for CH_3Br and 0.5 kcal/mol for CH_3I. The spin−orbit term does not add to the energy of the closed shell molecule CH_3X. There is however a contribution to ΔE_{SO} from the separated free halogen atoms[35] due to the spin−orbit splitting of the nonrelativistic ^2P ground state into the $^2P_{3/2}$ and $^2P_{1/2}$ components. The atomic splitting gives rise to

$$\Delta E_{SO} = E(^2P) - E(^2P_{1/2}) = {}^1/_3[E(^2P_{3/2}) - E(^2P_{1/2})] \tag{11}$$

which we have taken from experimental[36] data. The experimental bond dissociation energies, ΔH_{298}^0, observed at 298 K were converted to 0 K by using the approximate relation[37]

$$D_0^0 = \Delta H_{298}^0 - \frac{5}{2}RT - \left[\left(\sum_j \frac{R\Theta v_j}{\exp(\Theta v_j/T) - 1}\right)_{prod} - \left(\sum_j \frac{R\Theta v_j}{\exp(\Theta v_j/T) - 1}\right)_{reat}\right] \tag{12}$$

where R is the gas constant and Θv_j is the jth vibtational temperature; the second term, $5/2(RT)$, is due to the PV work contribution as well as the translational energy changes; the last term in eq (12) is the vibrational contribution to $\Delta H_T^0 - \Delta H_0^0$. The D_0^0 values from eq 12 are given in Table 3.

It is clear from Table 3 that the HF method underestimates the bond dissociation energies by up to 62% due to the neglect of electron correlation. The errors are largely reduced by partially including correlations in the MPn methods. However, the $F-CH_3$ and $Cl-CH_3$ bond energies are still underestimated by 3.6−10 kcal/mol in the MP2 and MP4 calculations, see Table 3. It appears that the electron correlation treatment is still inadequate at the MP2 and MP4 level of theory[29a] for the CH_3X

(34) Chase, M. W., Jr.; Davies, C. A.; Downey, J. R., Jr.; Frurip, D. J.; McDonald, R. A.; Syverud, A. N. *JANAF Theromdynamic Tables*, 3rd ed.; American Chemical Society: Washington, DC, 1985.

(35) (a) Balasubramanian, K.; Pitzer, K. S. *J. Chem. Phys.* **1983**, *78*, 321. (b) Christiansen, P. A.; Pitzer, K. S. *J. Chem. Phys.* **1981**, *74*, 1162. (c) Hafner, P.; Habitz, P.; Ishikawa, Y.; Wechsel-Trakowski, E.; Schwarz, W. H. E. *Chem. Phys. Lett.* **1981**, *80*, 311.

(36) Moore, C. E. *Atomic energy levels*; National Bureau Standards Circular 467: Washington, DC; Vol. I, 1949; Vol. II, 1952; Vol. III, 1958.

(37) For X = F and Cl, experimental correction terms from ref 34 were used to bring the experimental bond dissociation energies (ΔH_{298}^0) measured at 298 to 0 K (D_0^0). The values of the correction terms were −1.546 and −1.497 kcal/mol for X = F and Cl, respectively. These values are in good agreement with the corresponding estimates of −1.546 and −1.482 kcal/mol obtained from eq 12.

Table 4. Geometrical Parameters for the Ion–Dipole Complexes and Transition States[a]

geometric parameters	F				Cl				Br			I		
	LDA[b]	NL-SCF[b]	MP2[c]	HF[c]	LDA[b]	NL-SCF[b]	MP2[c]	HF[c]	LDA[b]	NL-SCF[b]	MP2[d]	LDA[b]	NL-SCF[b]	MP2[d]
Ion–Dipole Complexes, $X^-\cdots CH_3X$ (C_{3v})														
$R_{CX}^<$	1.443	1.471	1.454	1.416	1.807	1.835	1.808	1.824	2.015	2.042	1.983	2.192	2.237	2.183
$R_{CX}^>$	2.341	2.456	2.627	2.674	2.976	3.098	3.266	3.367	3.041	3.251	3.361	3.287	3.418	3.602
R_{CH}	1.094	1.090	1.084	1.074	1.093	1.089	1.084	1.073	1.091	1.090	1.080	1.092	1.089	1.080
∠HCX	109.1	108.2	107.7	108.1	109.6	107.9	108.9	108.0	107.3	106.4	107.5	107.8	106.2	107.3
Transition States, $[X\cdots CH_3\cdots X]^-$ (D_{3h})														
R_{CX}	1.791	1.855	1.836	1.846	2.279	2.342	2.316	2.394	2.443	2.512	2.461	2.664	2.726	2.670
R_{CH}	1.083	1.081	1.074	1.061	1.080	1.080	1.072	1.062	1.080	1.081	1.070	1.082	1.082	1.071

[a] See Figure 1 for a definition of geometrical parameters; distances in angstroms; angles in degrees. [b] This work, TZ+2P basis set. [c] X = F, Cl, ref 10b, 6-31++G(d,p) basis set. [d] This work, CEP-31++G(d) basis for Br and I; 6-31G(d,p) basis set for C and H.

systems. It is interesting to note that the MP2 bond energies are in better agreement with experiment than the MP4 estimates for the CH_3X systems, Table 3. It is possible that the error due to lack of electron correlation in the MP2 method is canceled by[38] errors due to the limited basis set applied in our ab initio studies. It is also important to note that ΔE_{SO} has a substantial contribution to the bonding energy. Thus, D_o^o is reduced by 7.2 kcal/mol for X = I and 3.5 kcal/mol for X = Br, Table 3. The same values for the ΔE_{SO} correction have been applied to the DFT and ab initio results.

We can draw two general conclusions by examining the DFT results in Table 3, both of which are in accordance with previous investigations.[11a,12] The first is that the LDA method overestimates bond energies, and the second is that the two different nonlocal correction schemes, NL-P and NL-SCF, provide essentially the same bond energies. It follows from Table 3 that the LDA method overestimates the bond energies by 20–25% whereas the NL bond energies are in better agreement with the experimental data than any other theoretical methods used in this study. The absolute errors for the four C–X bond energies are all less than 2.5 kcal/mol in the case of the NL-SCF scheme. We shall in a later section discuss the factors responsible for the variation in the $X-CH_3$ bond energies as a function of X.

We have seen that relativistic effects are of minor importance for the geometry and electron density of the closed shell CH_3X systems. Our QR calculations on the frequencies of CH_3I revealed that relativity has a minor influence on the force field of CH_3X as well. The largest change induced by relativity was a shift in the C–I stretching frequency of 17 cm^{-1}. We shall in the next section assume[35c] that relativistic effects can be neglected for the closed shell transition states and ion–dipole complexes as well.

B. Geometrical Structures, Vibrational Frequencies of the Ion–Dipole Complexes, and the Transition States. Table 4 displays the geometrical parameters for the ion–dipole complexes and the transition states. The structures presented in Table 4 were optimized at different levels of DFT and ab initio theory.

The key geometrical parameters in the ion–dipole complex $X^-\cdots CH_3X$ are the distance, R_{CX}, between the nucleophile, X^-, and the carbon center on the substrate, CH_3X, as well as the C–X distance, $R_{CX}^<$, of the CH_3X substrate itself. It follows from Table 4 that $R_{CX}^>$ and $R_{CX}^<$ depend strongly on the level of theory. The calculated order for $R_{CX}^>$ is LDA < NL-SCF < MP2 < HF. We shall shortly show that the calculated stability of the $X^-\cdots CH_3X$ complex follows the reverse order.

Boyd and co-workers[10b,39] have demonstrated that the HF method could inherently underestimate the covalent part of the bonding in $X^-\cdots CH_3X$ by tying the electron density on either X^- or CH_3X. The result is a weak complex and a long $R_{CX}^>$ distance. The tendency of the HF method to underestimate the covalent part of the bond between weakly interacting fragments has been analyzed by Buijse and Baerends.[40] The MP2 scheme decreases the $R_{CX}^>$ distance slightly. However, the electron density is still localized largely on the two interacting fragments.

Methods based on density functional theory do not suffer from the same bias toward charge localization in bonds between weakly interacting species. This point has been discussed by Tschinke and Ziegler.[41] Thus, the $R_{CX}^>$ bond distances calculated by the LDA and NL-SCF schemes are shorter than the ab initio counterparts, and both DFT-based methods afford a covalent component to the $X^-\cdots CH_3X$ bond. The LDA method tends to overestimate bond energies in comparison with experiment and the NL-SCF scheme. Thus, it is not surprising that the LDA scheme affords $R_{CX}^>$ distances that are shorter than the NL-SCF estimates.

A comparison between the transition state structures in Table 4 and the reactant geometries in Table 1 reveals that all levels of theory predict an increase in the C–X transition state bond length of about 30% for X = F and Cl and about 26% for X = Br and I. Also, the MP2 C–X bond distances for the transition state lie between the LDA and NL-SCF estimates for all four species. It follows further from Tables 4 and 1 that the C–H bond length decreases from the free CH_3X species to the transition states by about 1.5–1.0% along the series X = F, Cl, Br, and I. This is understandable since the C–H bonds in the transition state with a sp^2 hybridization are expected to have more 2s(C) participation than the C–H bonds in the isolated CH_3X species with a sp^3 hybridization.

The calculated harmonic vibrational frequencies for the ion–dipole complexes and the transition states are listed in Table 5. The vibrational calculations were based on the MP2 scheme or the LDA method. Also compiled in Table 5 are the scaled MP2 frequencies, where the scaling factor of $\eta = 0.94$ was that used by Trucker and Truhlar[10e] to reproduce the experimental fundamental frequencies for CH_3Cl. The data in Table 5 confirm that the ion–dipole complexes correspond to minimum points on the potential energy surfaces, while the transition states, as expected, represent first-order saddle points.

The two lowest frequencies of the ion–dipole complexes correspond to respectively a $X^-\cdots C-X$ bending mode of e symmetry and a $X^-\cdots C$ stretching mode of a_1 symmetry. We note that the LDA scheme affords higher frequencies for both modes than the MP2 method. This is in accordance with the fact that the LDA method provides a shorter (and stronger) bond between X^- and CH_3X than the MP2 scheme. The remaining

(38) Frisch, M. J.; Binkley, J. S.; Schaefer, H. F., III. *J. Chem. Phys.* **1984**, *81*, 1882.

(39) (a) Wang, J.; Eriksson, L. A.; Boyd, R. J.; Shi, Z.; Johnson, B. G. *J. Phys. Chem.* **1994**, *98*, 792. (b) Shi, Z.; Boyd, R. J. *J. Am. Chem. Soc.* **1991**, *113*, 1072.

(40) Buijse, M.; Baerends, E. J. *J. Chem. Phys.* **1990**, *93*, 4129.

(41) Tschinke, V.; Ziegler, T. *J. Chem. Phys.* **1990**, *93*, 8051.

Table 5. Vibrational Frequencies (cm^{-1}) of the Ion−Dipole Complexes and the Transition States

vibrational modes	F			Cl			Br			I		
	LDA[a]	MP2[b]	scaled[c]	LDA[a]	MP2[d]	scaled[e]	LDA[a]	MP2[f]	scaled[c]	LDA[a]	MP2[f]	scaled[c]
Ion−Dipole Complexes, $X^-\cdots CH_3X$												
$\omega_1(e/a_1)$[g]	176	94	88	89	72	68	89	64	60	70	46	43
$\omega_2(a_1/e)$[g]	245	165	155	140	114	107	102	84	79	85	72	67
$\omega_3(a_1)$	815	906	851	616	695	695	435	554	521	413	484	455
$\omega_4(e)$	1016	1114	1047	904	1033	971	853	995	935	812	928	872
$\omega_5(a_1)$	1232	1387	1304	1204	1396	1312	1138	1351	1270	1120	1315	1236
$\omega_6(e)$	1367	1522	1431	1376	1520	1428	1365	1515	1424	1367	1507	1416
$\omega_7(a_1)$	3011	3172	2982	3015	3225	3031	3023	3202	3010	3021	3198	3006
$\omega_8(e)$	3115	3303	3105	3125	3356	3154	3155	3360	3158	3153	3357	3155
Transition States, $[X\cdots CH_3\cdots X]^-$												
$\omega_1(a_2'')$	446i	590i	554i	401i	516i	485i	318i	449i	422i	308i	407i	382i
$\omega_2(e'/a_1')$[h]	348	357	335	206	219	206	141	145	136	77	107	100
$\omega_3(a_1''/e')$[h]	381	363	341	225	234	220	172	179	168	148	151	142
$\omega_4(e'')$	1062	1043	980	881	1007	946	847	980	921	815	931	875
$\omega_5(a_2'')$	1161	1176	1105	938	1086	1021	886	1039	977	816	960	902
$\omega_6(e')$	1268	1454	1367	1307	1469	1381	1309	1471	1383	1313	1470	1382
$\omega_7(a')$	3098	3204	3012	3094	3304	3106	3096	3273	3077	3085	3260	3064
$\omega_8(e')$	3253	3411	3206	3289	3520	3309	3293	3504	3294	3282	3495	3285

[a] This work, TZ+2P basis set, and the LDA geometries. [b] This work, 6-31G(d,p) basis set, MP2/6-31++G(d,p) geometries taken from ref 10b. [c] The scaled MP2 frequencies with a scaling factor of $\eta = 0.94$ as suggested in ref 10e. [d] Reference 10e, 6-31G(d,p) basis set and the MP2 geometries. [e] Reference 10e, the scaled MP2 frequencies with a scaling factor $\eta = 0.94$. [f] This work, 6-31G(d,p) basis set for C and H; CEP-31++G(d) basis for Br and I; the MP2 geometries. [g] In ω_1, e symmetry for X = F and Cl, a_1 symmetry for X = Br and I. In ω_2, a_1 symmetry for X = F and Cl, e symmetry for X = Br and I. [h] In ω_2, e′ symmetry for X = F and Cl, a_1' symmetry for X = Br and I. In ω_3, a_1' symmetry for X = F and Cl, e′ symmetry for X = Br and I.

frequencies in the ion−dipole complex refer to the CH_3X fragment. For these frequencies the MP2 values are larger than the LDA estimates, just as in the case of the free CH_3X molecule, Table 2. However, the scaled MP2 frequencies of the CH_3X fragment are in good agreement with the LDA values.

For the imaginary frequencies of the transition states, the MP2 values are much higher than the LDA estimates in absolute terms. This would imply that the DFT schemes provide potential energy surfaces around the transition states that are more shallow than those obtained by the MP2 method. We shall see in the next section that this is consistent with the fact that the DFT methods afford lower activation energies than the MP2 and MP4 schemes. The remaining parts of the transition state frequencies are all real, and the MP2 estimates are all higher than the LDA values, whereas the scaled MP2 frequencies are in line with the LDA data.

Cyr et al.[6a] have recently isolated a $I^-\cdots CH_3I$ complex in the gas phase and characterized it using negative ion photoelectron spectroscopy. They found that the C−I bond in the CH_3I fragment was elongated by 0.068 ± 0.005 Å and the H−C−I bond angle reduced by 1.9 ± 0.5° relative to the free CH_3I molecule. The DFT results are in good agreement with the experimental values. The calculated increases in the C−I bond length are 0.077 Å (LDA) and 0.081 Å (NL-SCF) whereas the estimated decreases in the H−C−I bond angle are 0.5° (LDA) and 1.1° (NL-SCF). The MP2 method predicts on the other hand a much smaller stretch of the C−I bond corresponding to 0.033 Å, whereas the decrease in the H−C−I bond angle is estimated as 0.4°. Furthermore, the LDA results predict the C−I stretching frequency of the CH_3X moiety to be reduced in the complex relative to the free molecule by 26%, which compared better with the experimental estimate (~20%)[6a] than the MP2 value (12%).

Hu and Truhlar[10g] have during the course of this work reported calculations on the structural distortion of CH_3I in the complex $I^-\cdots CH_3I$ at the MP2 and QCISD(T) levels. Our MP2 results are similar to those of Hu and Truhlar. However, the DFT results are closer to and compare better with experimental data than the best ab initio prediction by Hu and Truhlar based on the QCISD(T) method.

C. Comparison of the Well Depths and Barrier Heights.

The well depth, ΔE_0^C, and barrier height, ΔE_0^B, of Figure 1 are the key parameters in the S_N2 gas-phase reaction. It is thus not surprising that they have been studied extensively by theoretical and experimental methods.

Previously theoretical studies have largely been confined to the computationally less demanding fluorine and chlorine systems. Shi and Boyd[10b] reported HF and MP2 results for X = F and Cl with a 6-31++G(d,p) basis set. They found that while the MP2 barrier was 6.7 kcal/mol lower than the HF counterpart for X = F, the MP2 scheme afforded a barrier 1.1 kcal/mol higher than HF for X = Cl. Vetter and Zülicke[10d] obtained similar results in an investigation based on multireference single- and double-excitation configuration interaction (MRSD-CI) calculations with a DZ2P basis and HF geometries. They concluded that electron correlation tends to reduce the barrier height for the first row system with X = F, whereas the opposite is the case for X = Cl and Br. Other authors[9a,42] have drawn similar conclusion. In the studies mentioned above all calculations were based on a limited DZ2P, or similar quality basis set.

Wladkowski et al.[10a] have recently studied the $Cl^- + CH_3Cl$ S_N2 reaction at the HF, MP2, and MP4 levels of theory with the most extensive basis set TZ3P+R+(2f,d) applied to date. Their results demonstrated that introducing electron correlation at the MP2 level reduces the barrier by 4.1 kcal/mol and that the barrier is lowered further by about 1.7 kcal/mol at the MP4 level of theory. Thus, the more exact calculations by Wladowski et al.[10a] seem to indicate that electron correlation lowers the barrier for the heavier elements as well, in accordance with what one might expect.[43]

We have carried out a systematic ab initio comparison of ΔE_0^C and ΔE_0^B for X = F, Cl, Br, and I by supplementing the accurate results of Wladkowski et al.[10a] in the case of X = Cl with studies based on basis sets of nearly the same accuracy for X = F, Br, and I. Energies were evaluated up to the MP4SDTQ level of theory whereas the geometries were

(42) Luke, B. T.; Loew, G. H.; McLean, A. D. *Int. J. Quantum Chem.* **1986**, *29*, 833.

(43) Harding, L. B. In *Advances in Molecular Electronic Structure Theory*; Dunning T. H., Jr., Ed.; JAI Press: Greenwich, CT, 1990; Vol. 1.

Table 6. Complexation Energies and Barrier Heights for the S_N2 Reaction $X^- + CH_3X = XCH_3 + X^-$ (X = F, Cl, Br, and I)[a]

	ΔE_0^C						ΔE_0^B					ΔE_0^{IB}				
halogen (X)	LDA[b]	NL-SCF[b]	HF[c]	MP2[c]	MP4[c]	exp[d,e]	LDA[b]	NL-SCF[b]	HF[c]	MP2[c]	MP4[c]	LDA[b]	NL-SCF[b]	HF[c]	MP2[c]	MP4[c]
F	−25.2	−19.9	−11.8	−13.1	−13.5		−18.0	−13.1	7.1	0.1	−2.5	7.2	6.8	18.9	13.2	11.0
Cl	−14.4	−10.3	−8.1	−10.5	−10.6	−8.6 ± 0.2	−8.9	−5.7	7.6	3.5	1.8	5.6	4.6	15.7	14.0	12.4
Br	−14.4	−10.4	−7.6	−8.7	−8.5	−9.2 ± 0.5	−11.5	−7.3	5.4	3.1	2.3	2.9	3.1	13.1	11.9	10.8
I	−11.1	−7.4	−6.4	−7.8	−8.3	−9.0 ± 0.2	−9.0	−5.6	5.2	2.3	0.9	2.1	1.8	11.6	10.1	9.2

[a] ΔE_0^C, ΔE_0^B, and ΔE_0^{IB}, in kcal/mol, are the vibrationless relative energies defined in eqs 2, 3, and 4, respectively. [b] This work, TZ+2P basis set; ΔZPE calculated from eq 9 by LDA frequencies. [c] For X = F, Br, and I, this work; for X = Cl, ref 10a. All *ab initio* results based on the MP2 geometries (see text). For X = F and Cl, TZ3P+R+(2f,d) basis set; for X = Br and I, 6-31G(d,p) basis set used for H and C atoms, and CEP-31++G(d) basis set used for Br and I atoms; ΔZPE calculated from eq 9 by MP2 frequencies. [d] Experimental ΔE_0^C values estimated from ΔH_{298}^C according to eq 12. [e] A more recent experimental value for the Cl system is $\Delta H_{298}^C = 12 \pm 2$ kcal/mol, ref 45.

optimized at the MP2 level. Exactly the same quality basis set, TZ3P+R+(2f,d), used by Wladkowski et al.[10a] for chlorine was employed in the present study for X = F, while a CEP-31++G(d) basis set was adapted for the Br and I atoms. The results are compiled in Table 6. Also listed in Table 6 are the corresponding DFT results based on the LDA and NL-SCF schemes along with experimental complexation energies. The NL-P energies are not included in Table 6, since they differ by less than a few tenths of a kilocalorie per mole from their NL-SCF counterparts.

We shall first examine the energy of formation for the ion−dipole complex given by the well depths ΔE_0^C of Figure 1, see Table 6. Earlier experimental measurements by high pressure mass spectrometry due to Dougherty et al.[44] showed that the enthalpy changes upon complexation at the average temperature 488 K are respectively −8.6 ± 0.2, −9.2 ± 0.5, and −9.0 ± 0.2 kcal/mol for the Cl, Br, and I systems. More recently, Larson and McMahon[45] used ion cyclotron resonance techniques to determine a standard complexation enthalpy of −12 ± 2 kcal/mol for $Cl^- + CH_3Cl$. The experimental values for ΔE_0^C (ΔH_0^C) can be estimated from the observed values of ΔH_{488}^C by using eq 12.

Our calculations indicate that ΔE_0^C happens to be nearly the same as ΔH_{488}^C for the all halogen systems since contributions from the second and third term in eq 12 cancel out. In the case of the chlorine system the LDA complexation energy is too large whereas the HF value on the other hand is too small compared to the most recent experimental estimate of −12 ± 2 kcal/mol. The NL-SCF scheme as well as the two correlated ab initio methods, MP2 and MP4, offer on the other hand results for the $Cl^-\cdots CH_3Cl$ complexation energy which fall in the region observed by Larson and McMahon,[45] Table 6.

For the bromine system, the NL-SCF scheme as well as the MP2 and MP4 methods estimate the stability of the complex, ΔE_0^C, to be higher than the one determined experimentally by Dougherty[44] et al., whereas the HF scheme reproduces the experimental date. It is possible that Dougherty et al.[44] have underestimated the $X^-\cdots CH_3X$ complexation energy for X = Br, as in the chlorine case.

When X = I, the NL-SCF, MP2, and MP4 results again compared better with the experimental date than the LDA and HF estimates. No experimental data are available for the fluorine system. As can be expected from the specific periodic properties of the fluorine atom, a large electronegativity and a small ionic radius, all the theoretical methods predict the complexation energy to be significantly larger than for X = Cl, Br, and I. However, the difference between the DFT estimates and the ab initio values is substantial, with the NL-SCF value exeeding the MP4 estimate by 6.4 kcal/mol. In view of the fact that the MP4 scheme underestimates the $F-CH_3$ bond energy by 10.9 kcal/mol whereas the NL-SCF overestimates the bond energy only by 0.8 kcal/mol (Table 3), we feel the NL-SCF predicted $F^-\cdots CH_3F$ binding energy to be more reliable.

The bonding in the $X^-\cdots CH_3X$ complex has been attributed to a pure ion−dipole interaction between X^- and CH_3X. In this bonding description electron correlation would play a secondary role for the stability of the complex. In fact, electron correlation was not found to add to the stability of the $X^-\cdots CH_3X$ complex in the series of ab initio calculations carried out by Vetter et al.[10d] Our calculations reveal on the other hand that the complexation energies are enhanced by electron correlation. Thus, the differences between the MP4 estimates and the corresponding HF results are as large as 2 kcal/mol, Table 6. Our results would indicate that orbital interactions as well as the purely ion−dipole electrostatic attraction are of importance for ΔE_0^C. We shall expand on this point in the next section. The trends in ΔE_0^C obtained by the different computational methods are summarized in Figure 2.

Compared to the complexation energies, ΔE_0^C, the barrier heights, ΔE_0^B, are much more difficult to determine accurately. Experimentally, only two direct measurements[3a,8] of the rate constants are available to date, both of them for the $Cl^- + CH_3Cl$ system. Unfortunately, it has only been possible to estimate the barrier ΔE_0^B of the $Cl^- + CH_3Cl$ system to within a few kilocalories per mole as a result of experimental uncertainties[3a,8] as well as approximations inherent in the theoretical model[10e] used to fit the experimental data. The most recent experiment was carried out by Barlow et al.[3a] using a tandem flowing afterglow-SIFT-Drift instrument and a modified method for kinetic analysis. In this experiment CH_3Cl is bombarded by Cl^- anions of a certain kinetic energy. Barlow et al.[3a] found a nearly constant reactivity for kinetic energies between 0.026 and 0.4 eV, whereas the rate constant rose exponentially for kinetic energies between 0.5 and 2.0 eV. It was concluded that the Cl exchange reaction takes place exclusively via the S_N2 channel illustrated in Figure 1 when the kinetic energy is below 0.4 eV. The barrier for this channel was estimated to be 1 ± 1 kcal/mol based on simple RRKM theory. The rate increase for kinetic energies between 0.5 and 2.0 eV was attributed to the onset of a new channel for the Cl exchange process:

$$Cl^- + CH_3Cl = [CH_3\cdot ClCl]^- = ClCH_3 + Cl^- \quad (13)$$

By using the model of translationally driven reactions,[46] Barlow et al. estimated the activation barrier for process 13 to be about 2.0 eV.[3a] We shall return to the reaction in eq 13 after we have completed the discussion of the S_N2 process.

It follows from Table 6 that the HF value for the S_N2 barrier, ΔE_0^B, is too high compared to the experimental estimate[3a] of 1

(44) (a) Dougherty, R. C.; Dalton, J.; Roberts, J. D. *Org. Mass Spectrum* **1974**, *8*, 77. (b) Dougherty, R. C.; Roberts, J. D. *Ibid.* **1974**, *8*, 81. (c) Dougherty, R. C. *Ibid.* **1974**, *8*, 85.

(45) Larson, J. W.; McMahon, T. B. *J. Am. Chem. Soc.* **1985**, *107*, 766.

(46) Chesnavich, W. J.; Bowers, M. T. *J. Phys. Chem.* **1979**, *83*, 900.

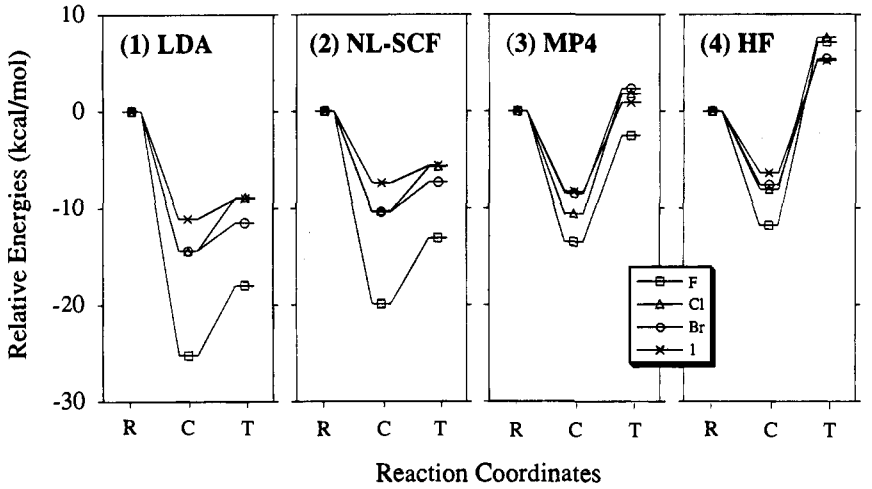

Figure 2. An overview of the potential energy surface for the gas-phase S_N2 reactions, $X^- + CH_3X = [X\cdots CH_3\cdots X]^- = CH_3X + X^-$ (X = F, Cl, Br, I), predicted by the different levels of theory; R, C, and T represent the reactants (products), ion–dipole complexes, and transition states, respectively.

± 1 kcal/mol in the case of the chlorine system. By contrast the corresponding LDA estimate is seen to be too low. The best fit to experiment is obtained by the MP4 scheme, whereas the MP2 value is about 2 kcal/mol too high and the NL-SCF estimate 6 kcal/mol too low. However, we note again that the experimental value for ΔE_0^B is uncertain by at least a few kilocalories per mole.[3a,10e]

We have tried to deduce an estimate for ΔE_0^B by substituting the experimental rate constant, k, as well as a calculated value for the activation entropy, $\Delta S^{\ddagger}$, into the Eyring formula:

$$k = \frac{\mathbf{k}T}{h}\exp\left(\frac{\Delta S^{\ddagger}}{R}\right)\exp\left(\frac{-\Delta H^{\ddagger}}{RT}\right) \qquad (14)$$

where $\mathbf{k}$ and h are the Boltzmann and Planck constants, respectively. Such a substitution makes it possible to find $\Delta H^{\ddagger}$ from which ΔE_0^B can be determined by eq 12. We obtained in this way a value of 0.4 kcal/mol for ΔE_0^B, in reasonable agreement with the estimate of 1 ± 1 kcal/mol due to Barlow et al.[3a]

The entropy calculations were based on LDA geometries and frequencies. The calculations revealed that the change in entropy upon formation of the ion–dipole complex from the reactants is −17.6 eu at 298 K, in good agreement with the experimental estimate of −15.3 ± 1.0 eu due to Dougherty et al.[44] The entropy of the transition state is −25.0 eu relative to the separated reactants. Thus, entropy factors are seen strongly to reduce the rate of the Walden inversion process. Based on the above discussion we infer that the MP4 values constitute the upper bound for the barrier heights of the S_N2 exchange reactions in eq 1 while the NC-SCF estimate provided the lower bound.

We shall now turn to a brief discussion of the S_N2 barrier, ΔE_0^B, for the remaining halogen systems with X = F, Br, and I. Absolute values for ΔE_0^B, are not known experimentally in the case of fluorine, bromine, and iodine. However, it has been established that the rates for the three heavier halogens qualitatively are similar.[8a] This is in line with the theoretical predictions in Table 6. Thus for any of the computational methods applied here the spread in the calculated ΔE_0^B values within the series X = Cl, Br, and I is less than 2 kcal/mol. We note further that ΔE_0^B is calculated to be lower for fluorine than for the heavier halogens. Finally, the DFT method provides negative barriers whereas the ab initio estimates are positive expect for X = F at the MP4 level. A general trend that can be drawn from Table 6 is that the barrier heights of all the S_N2 reactions in eq 1 predicted by different levels of theory are in the order LDA ≪ NL-SCF ≪ MP4 < MP2 ≪ HF.

It is also interesting to compare calculated trends in the intrinsic barriers, ΔE_0^{IB}, obtained by the different theoretical schemes. We note that the intrinsic barriers calculated by the DFT-based methods are lower than those due to ab initio techniques. Among the ab initio methods the barrier for a particular system is seen to diminish from the HF estimates as more and more electron correlation is included via the MP2 and MP4 calculations, in accordance with what one might expect.[43] The trends in ΔE_0^{IB} and ΔE_0^B obtained by the different computational methods are summarized in Figure 2.

D. Intrinsic Reaction Pathways for the S_N2 Process as Well as the Alternative Exchange Channel. We have explored the potential energy surface of the $X^- + CH_3X$ reaction system in more detail by tracing the intrinsic reaction pathways (IRPs) for the S_N2 process as well as the alternative[3a] exchange channel of eq 13 in the case of X = Cl. The IRP follows a reaction from the transition state along the direction corresponding to the imaginary vibrational mode in a steepest descend fashion toward the reactants (products). The IRP calculations were carried out at the NL-P level of theory in mass-weighted internal coordinates without symmetry constraints.[12a]

Figure 3 displays the geometrical transformations along the IRP for the S_N2 process, $Cl^- + CH_3Cl = [Cl\cdots CH_3\cdots Cl]^- = ClCH_3 + Cl^-$. The reaction starts at the minimum for the ion–dipole complex, Figure 3a, and the initial stages of the S_N2 process constitute a shortening of the $X^-\cdots C$ bond distance while the other geometrical parameters essentially are kept unchanged, Figure 3a–c. The second part of the Walden inversion process, Figure 3d–h, represents a further contraction of the $X^-\cdots C$ bond distance in concert with a C–X bond elongation and a synchronous increase in the ∠HCX⁻ angle. The C–H bond length is further seen to contract from 1.09 Å in the complex to 1.08 Å in the transition state. The overall geometrical transformation in Figure 3 is in line with our previous study on the S_N2 reaction for the $H^- + CH_4$ system[12a] in which the IRP calculation was carried out under C_{3v} symmetry constraint. That is, the umbrella pops open gradually during the inversion process rather than abruptly at the end toward the transition state.

The optimized transition state structure for the alternative chlorine exchange reaction[3a] of eq 13 is given in Figure 4. The structure was optimized by DFT and ab initio methods. It follows from the comparison in Figure 4 that the DFT methods and the MP2 scheme afford similar transition state structures

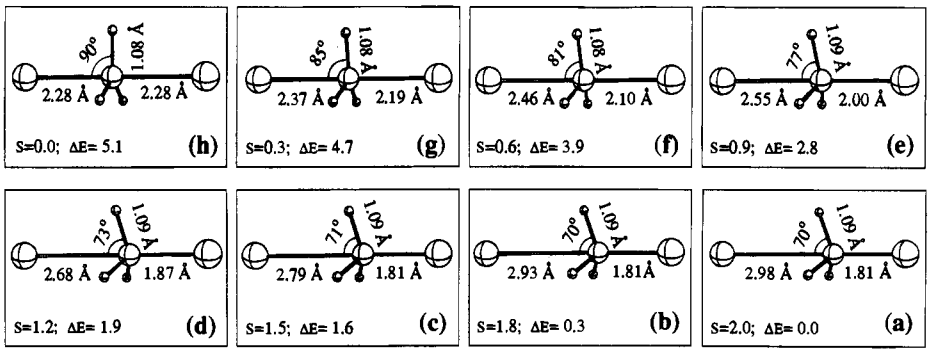

Figure 3. Atomic movements during the S_N2 reaction, $CH_3Cl + Cl^- = [ClCH_3Cl]^- = CH_3Cl + Cl^-$, based on the IRP calculation at the LDA level. The balls in order of size from large to small represent chlorine, carbon, and hydrogen atoms, respectively. The length s of the IRP is in amu$^{1/2}$·bohr. The point $s = 0.0$ corresponds to the transition state; ΔE in kcal/mol is the electronic energy relative to the complex, $Cl^-\cdots CH_3Cl$, calculated by the NL-P scheme. No symmetry constrain was employed in the IRP calculation.

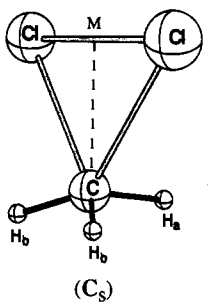

R(C-H_a)	1.069	HF/6-31G**			
	1.075	MP2/6-31G**			
	1.088	LDA/TZ+2P			
	1.085	NL-SCF/TZ+2P			
R(C-H_b)	1.066	R(C-M)	1.818	R(Cl-Cl)	4.112
	1.075		1.773		3.268
	1.088		1.779		3.314
	1.083		1.872		3.624
∠MCH_a	85.2	∠MCH_b	97.4	∠H_bMCH_a	118.0
	95.9		109.5		118.2
	94.3		107.2		117.9
	92.9		101.9		118.6

Figure 4. The transition state structure predicted by the DFT and ab initio methods at different levels of theory for the chlorine exchange reaction, $CH_3Cl + Cl^- = [CH_3ClCl]^- = CH_3Cl + Cl^-$. M is the midpoint of the Cl−Cl bond; bond lengths are in angstroms, and bond angles are in degrees.

with a relatively short Cl−Cl distance. The HF scheme yields on the other hand a looser transition state structure with a larger Cl−Cl separation. The calculated transition state frequencies were 479i(a″), 137(a′), 169(a″), 355(a′), 692(a′), 776(a″), 999-(a′), 1328(a″), 1372(a′), 3024(a′), 3153(a″), and 3186(a′) at the LDA level and 689i(a″), 56(a′), 111(a″), 340(a′), 584(a″), 594-(a′), 1242(a′), 1550(a″), 1572(a′), 3389(a′), 3587(a′), 3591(a″) at the MP2 level. These results confirm the transition state of Figure 4 is a first-order saddle point on the potential energy surface.

The geometrical changes along the IRP for the alternative chlorine exchange reaction[3a] of eq 13 are displayed in Figure 5. The reaction starts as in the S_N2 case at the minimum for the ion−dipole complex, Figure 5a. In the S_N2 process Cl^- moved along the C_3 axis toward the carbon center, Figure 3a−d. In the alternative chlorine exchange reaction[3a] of eq 13, Cl^- proceeds perpendicular to the C_3 axis toward one of the CH_3Cl hydrogens to form a $Cl^-\cdots H$ bond, Figure 5a−d. In the second stage, the Cl^- anion moves toward Cl of the methyl chloride until a $Cl^-\cdots Cl$ distance of round 3.3 Å has been reached, Figure 5e−h. At this stage a $Cl^-\cdots H$ separation of about 2.1 Å and a C−Cl distance around 1.77 Å are maintained as part of the evolving Cl−C−H−Cl^- four-center activated structure. The final steps, Figure 5i−l, represent a synchronous movement of the two chlorine atoms and the re-orientation of the methyl group to elongate the C−Cl bond and reduce the C−Cl^- separation as well as to break the $Cl^-\cdots H$ hydrogen bond until the three-center transition state has been formed.

The activation energy for the process in eq 13 is calculated to be 61.9, 55.3, and 51.5 kcal/mol by the HF, MP2, and MP4 schemes, respectively. In the ab initio calculations use was made of a 6-311++G(d,p) basis set as well as the MP2 geometries with MP2 vibrational zero-point energy (ZPE) corrections. The corresponding DFT-based activation energies were 31.0, and 34.1 kcal/mol for the LDA and NL-SCF schemes, respectively, with inclusion of the LDA ZPE correction. Thus, the DFT methods underestimate the experimental barrier of 46 kcal/mol,[3a] whereas the ab initio barriers are too high. It seems to be a general trend that ab initio methods and

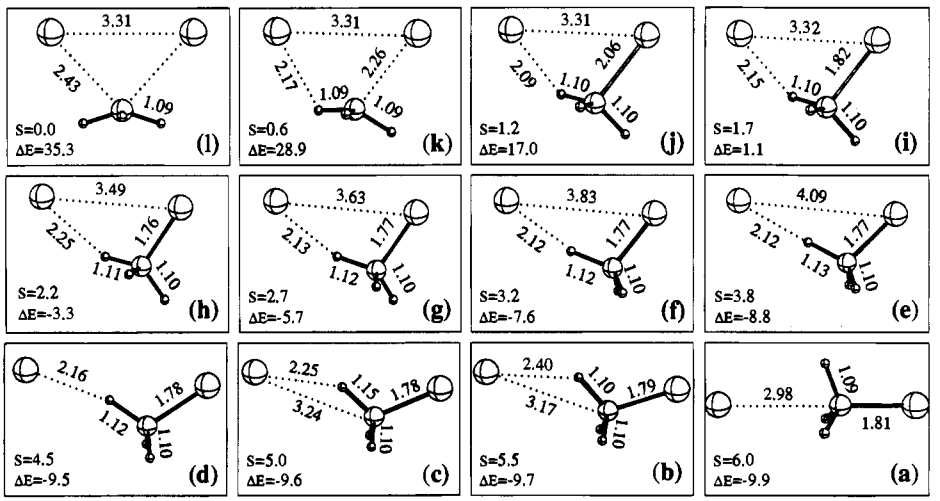

Figure 5. Atomic movements for the chlorine exchange reaction, $CH_3Cl + Cl^- = [CH_3ClCl]^- = CH_3Cl + Cl^-$, based on the IRP calculation at the LDA level. The balls in order of size from large to small represent chlorine, carbon, and hydrogen atoms, respectively. The length s of the IRP is in amu$^{1/2}$·bohr. The point $s = 0.0$ corresponds to the transition state; ΔE in kcal/mol is the electronic energy relative to the separated reactants (products), $Cl^- + CH_3Cl$, calculated by the NL-P scheme.

Table 7. Decomposition Analyses of the X−C Bond Energies (kcal/mol) for the $X-CH_3$, $X^-\cdots CH_3X$, and $[X\cdots CH_3\cdots X]^-$ with X = F, Cl, Br, and I[a]

ΔE_{BD} and components		F	Cl	Br	I
Reactants, $X-CH_3$ (C_{3v})					
ΔE_{steric}		152.0	85.6	55.8	45.0
ΔE_{orbit}		−277.9	−179.0	−137.0	−115.4
ΔE_{prep}		6.5	5.9	5.4	5.2
ΔE_{BD}		119.4	87.5	75.8	65.2
Ion−Dipole Complexes, $X^-\cdots CH_3X$ (C_{3v})					
ΔE_{steric}		−3.7	−2.8	−3.0	−1.0
ΔE_{orbit}	a_1	−11.5	−5.9	−6.5	−7.3
	e	−6.3	−2.6	−1.8	−1.6
	total	−17.8	−8.5	−8.3	−8.9
ΔE_{prep}		1.7	0.5	0.5	0.3
ΔE_{BD}		19.8	11.7	11.8	9.7
Transition States, $[X\cdots CH_3\cdots X]^-$ (D_{3h})					
ΔE_{steric}		78.4	39.5	29.8	24.2
ΔE_{orbit}		−162.2	−99.3	−82.6	−70.0
ΔE_{prep}		−51.0	−34.2	−30.5	−26.6
$(1/2)\Delta E_{BD}$		67.4	47.0	41.7	36.1

[a] The electronic energies at the level of NL-P//NL-SCF.

DFT schemes provide respectively upper and lower bounds to the actual barrier.[12]

The potential energy surface for movements of Cl^- at large and constant $Cl^-\cdots CH_3Cl$ separations is very soft, Figure 5a−d. It is thus possible that the reaction in eq 13 can be initialized by the Cl^- anion attacking on either the face or edge sites of the substrate CH_3X. The S_N2 reaction requires on the other hand a more restricted face approach along a C_3 axis.

E. Bond Energy Decomposition and Population Analyses. We shall finally in this section apply the ETS method[26] to an energy decomposition analysis of the X−C bond strength in the reactants, the ion−dipole complexes, and the S_N2 transition states. Our goal is to provide insight into the factors of importance for the X−C bond strength. The ETS method will also be used to rationalize trends in the X−C dissociation energies with respect to the different halogens.

It is straightforward to specify the fragments involved in the $X-CH_3$ bond formation of the reactant, CH_3X

Scheme I

$$X^\bullet + {}^\bullet CH_3 \rightarrow X-CH_3$$

or the $X^-\cdots CH_3X$ adduct bond of the ion−dipole complex,

Scheme II

$$X^- + CH_3X \rightarrow X^-\cdots CH_3X$$

For the purpose of analyzing the bonds in the transition states, we consider the formation of $[X\cdots CH_3\cdots X]^-$ from X^-, $^\bullet X$, and $^\bullet CH_3$ in two steps as illustrated in Scheme III.

Scheme III

$$X^\bullet + X^- + CH_3 \rightarrow [X\cdots X]^- + {}^\bullet CH_3 \rightarrow [X\cdots CH_3\cdots X]^-$$

In the first step, X^- and $^\bullet X$ are combined into the fragment $[X\cdots X]^-$, with the $X\cdots X$ separation kept the same as in the transition state. Further, the $^\bullet CH_3$ fragment is relaxed to the geometry of the CH_3 framework of the transition state. The energy change of the system in this step accounts for the preparation energy, ΔE_{prep}. In the second step, the two fragments are combined to form the $[X\cdots CH_3\cdots X]^-$ bond.

Table 7 compiles the results of the ETS bond energy decomposition calculations, where the preparation energy in Scheme I is the energy required to deform the CH_3 fragment from its planar D_{3h} conformation to the trigonal pyramidal C_{3v} geometry of the CH_3 framework in the molecule, CH_3X. For Scheme II, ΔE_{prep} represents the distortion energy of a free CH_3X molecule to the CH_3X structure in the ion−dipole complex. A general observation of Table 7 is that the orbital interaction energy, ΔE_{orbit}, is the dominant contributor to the X−C bond energy for Schemes I−III. Further, the trends in the X−C bond strengths for different halogens follow in all cases that of ΔE_{orbit}, whereas the much smaller contributions from ΔE_{steric} and ΔE_{prep} might enhance or oppose the general trend.

We will start with a discussion of the $X-CH_3$ bond of Scheme I. It follows from Table 7 that ΔE_{prep} is small in absolute terms and without any significant influence on the trend in the $X-CH_3$ bond energies. The trend is set by the orbital interaction term, ΔE_{orbit}, which gives rise to the order of $F \gg Cl > Br > I$ in the $X-CH_3$ bond strength. The steric interaction energy, ΔE_{steric}, tends to reduce the bond strength. It is numerically smaller than ΔE_{orbit} and runs counter to the order imposed by ΔE_{orbit}, Table 7.

The dominant term in the steric energy contribution, ΔE_{steric}, is due to the Pauli repulsion, ΔE_{Pauli}, between occupied spin orbitals on the $X^\bullet$ and $^\bullet CH_3$ fragment of the same spin polarization. Of particular importance is the interaction between the p_σ orbital on X and the 2s(C) based C−H σ-bonding orbital on $^\bullet CH_3$ of A_1 symmetry as well as the interaction between the two p_π halogen orbitals and the $2p_\pi$(C) based C−H σ-bonding orbitals on $^\bullet CH_3$ of E symmetry. The decrease in ΔE_{Pauli} from F to I is related to a similar reduction in overlaps between occupied spin orbitals on the $X^\bullet$ and $^\bullet CH_3$ fragments.

The orbital interaction energy, ΔE_{orbit}, as listed in Table 7, is due mainly (>92%) to the two-electron two-orbital interaction between the SOMOs of the $^\bullet CH_3$ and $X^\bullet$ fragments, $2p_\sigma^1$(C) and np_σ^1(X) of different spin, see Figure 6. Our calculations show that the overlaps between these two orbitals, S_{bond}, are in the order opposite to that of ΔE_{orbit} and ΔE_{BD} with 0.261, 0.341, 0.348, and 0.355 for X = F, Cl, Br, and I, respectively. The overlap trend might at first sight seem surprising[47] since np_σ on X becomes more diffuse in going from F to I. However, the overlap S_{bond} is determined by the extent of the np_σ orbital in relation to the C−X distance and the latter is determined strongly by the Pauli repulsion term, ΔE_{Pauli}. That is, any decrease in the C−X distance that would enhance S_{bond} will normally also increase ΔE_{Pauli}. For fluorine the π-type repulsion between p_π halogen orbitals and the $2p_\pi$(C) based C−H σ-bonding orbitals on $^\bullet CH_3$ increases steeply toward shorter C−F distances since the orbitals involved have the same radial extent. Thus S_{bond} is barred from reaching its optimal value. For chlorine and the heavier halogens the π-type repulsion becomes less sever and it becomes possible to reach X−C equilibrium distances that are more optimal for S_{bond}. The situation is very similar to that observed among the dihalogens where the F_2 bond is weaker than that of Cl_2 due to the strong repulsion between p_π lone pairs in the fluorines.

For the purpose of deciphering the trend of ΔE_{orbit} and ΔE_{BD}, we carried out a Mulliken population analysis on the $3a_1$ MO (corresponding to the σ_{X-CH_3} bond) of the molecule CH_3X, see Figure 6, in terms of the $^\bullet CH_3$ and $X^\bullet$ fragment orbitals. The results reveal that ΔE_{orbit} correlates[48] to the amount of electron density, ΔN, transferred from $^\bullet CH_3$ to $X^\bullet$. We calculate ΔN as 0.233 (F), 0.166 (Cl), 0.128 (Br), and 0.104 (I). A plot, Figure 7, of ΔN against ΔE_{orbit} and ΔE_{BD} reveals a linear relationship

(47) Rauk, A. *Orbital Interaction Theory of Organic Chemistry*; Wiley: New York, 1994.

(48) (a) Fujimoto, H.; Satoh, S. *J. Phys. Chem.* **1994**, *98*, 1436. (b) Pearson, G. R. *J. Am. Chem. Soc.* **1985**, *107*, 6801.

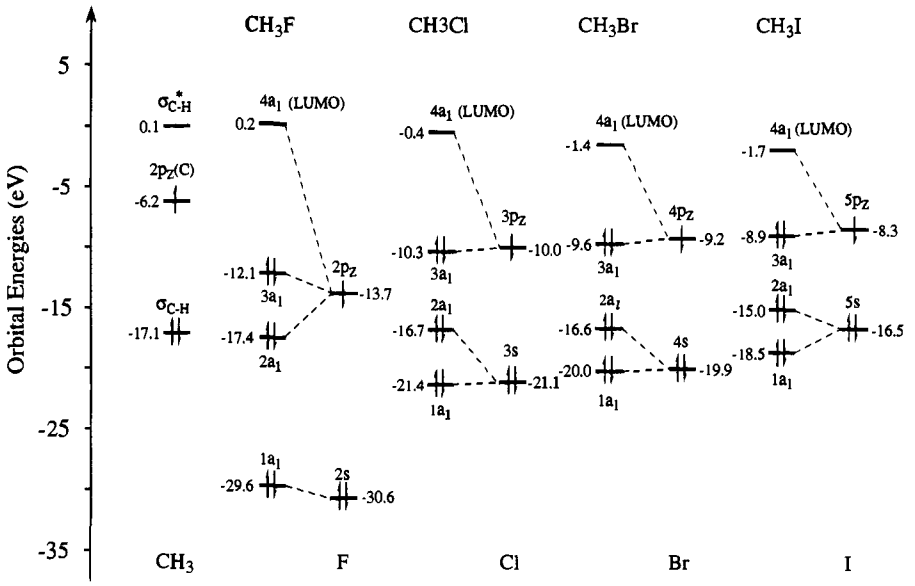

Figure 6. Interaction diagrams of the A_1 symmetry orbitals between the $^{\bullet}CH_3$ and $^{\bullet}X$ fragments in methyl halides, CH_3X, with X = F, Cl, Br, and I.

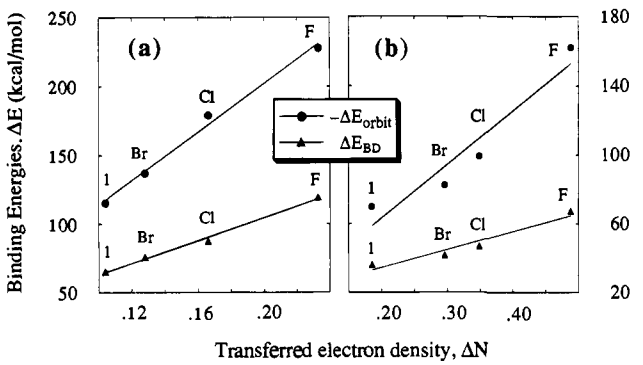

Figure 7. A diagram correlating the amount of electron density transfer from CH_3 to X, ΔN, with the binding energy ΔE_{BD} and the orbital interaction term ΔE_{orbit}. The points represent F, Cl, Br, and I systems, respectively, in the order of increasing ΔN. (a) For the reactants, $X-CH_3$; (b) For the transition states, $[X^{\bullet}\cdots{}^{\bullet}CH_3\cdots X]^-$.

with correlation coefficients of respectively 0.996 and 0.997. Thus the X–C bond is enhanced by a large electronegativity difference[48] between C and X and a corresponding large CH_3 to X charge transfer.

The term ion–dipole complex for the $X^-\cdots{}^{\bullet}CH_3X$ adduct might indicate that is primarily is kept together by the electrostatic interaction between the X^- and CH_3X fragments. However, we shall show that orbital interactions in the form of charge transfers from X^- to CH_3X are of equal importance for the stability of $X^-\cdots{}^{\bullet}CH_3X$. The ETS bonding analysis shows that the Pauli repulsion term, ΔE_{Pauli}, is negligible and that the steric interaction, ΔE_{steric} in Table 7, is dominated by the ion–dipole electrostatic interaction, ΔE_{elst}, between the fragments X^- and CH_3X. Further, ΔE_{steric} is seen to decrease in absolute terms from fluorine to iodine as the $X^-\cdots{}^{\bullet}CH_3X$ distance, and hence the ion–dipole interaction ΔE_{elst}, decreases. The term $-\Delta E_{steric}$ adds to the stability of the complex and follows the same trend as the total complexation energy, ΔE_{BD}, of the complex. However, it represents only 15 to 25% of the total bond energy ΔE_{BD}, Table 7.

The major part of ΔE_{BD} comes from the orbital interaction term ΔE_{orbit}. Of particular importance here is the charge transfers from $np_\sigma(X^-)$ to $4a_1(CH_3X, \sigma^*_{C-X})$ and $5a_1(CH_3X, \sigma^*_{C-H})$, Figure 8a, and from $np_\pi(X^-)$ to $2e(CH_3X, \sigma^*_{C-H})$, Figure 8b,c. A Mulliken population analysis revealed that the amount of electron transfer from X^- to CH_3X is 0.140, 0.095, 0.109, and 0.136 due to the a_1 symmetry orbital interaction, Figure 8a, and 0.072, 0.033, 0.022, and 0.020 owing to the e symmetry orbital interactions, Figure 8b,c, for X = F, Cl, Br, and I, respectively. The trend in the total charge transfer, ΔN, can readily be understood from the variation in the electronegativity of X in the CH_3X molecule. The trend is further in accord with the order calculated for ΔE_{orbit} and hence ΔE_{BD}, Table 7, and ΔN represents the driving force behind the $X^-\cdots{}^{\bullet}CH_3X$ complex formation with a contribution of between 75 and 85% to ΔE_{BD}.

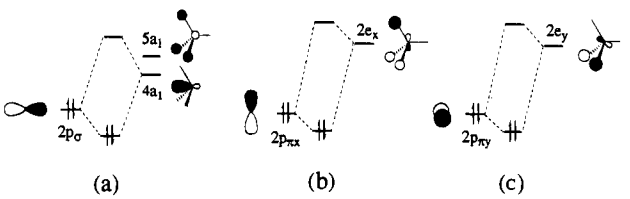

Figure 8. The orbital interaction diagrams for the formation of the ion–dipole complex $X^-\cdots{}^{\bullet}CH_3X$ with X = F, Cl, Br, and I.

We shall finally turn to a discussion of the transition state. We find that the binding energy, ΔE_{BD}, for the transition state $[X^{\bullet}\cdots{}^{\bullet}CH_3\cdots X]^-$ with respect to the X^-, $^{\bullet}X$, and $^{\bullet}CH_3$ fragments, Scheme III, decreases from fluorine to iodine, Table 7, in line with the corresponding trends found for Schemes I and II. The term ΔE_{orbit} is the dominant contributor to ΔE_{BD} in the case of the transition state, Table 7. The orbital energy term ΔE_{orbit} is primarily (>90%) the result of the interaction between $2p_\sigma$ on the planar CH_3 framework and an out-of-phase np_σ combination on the $[X^{\bullet}\cdots X]^-$ fragment, Figure 9. Both fragment orbitals hold a single unpaired electron and the interaction results in one fully occupied bonding orbital, $1a_2''$ of Figure 9. The term $-\Delta E_{orbit}$ is seen to decrease from fluorine to iodine just as in the case of CH_3X and the ion–dipole complex $X^-\cdots{}^{\bullet}CH_3X$.

The driving force for formation of the $[X^{\bullet}\cdots{}^{\bullet}CH_3\cdots X]^-$ bond is the electron density transfer, ΔN, from $^{\bullet}CH_3$ to $[X^{\bullet}\cdots X]^-$, which primarily takes place in the a_2'' symmetry representation, Figure 9. The charge transfer, ΔN, arising from the interaction between the two a_2'' symmetry orbitals, Figure 9, is 0.488, 0.349, 0.296, and 0.186, respectively, for X = F, Cl, Br, and I. A correlation between ΔN and ΔE_{orbit} as well as ΔE_{BD} is shown in Figure 7b. The corresponding correlation coefficients are 0.956 and 0.968, respectively. The charge transfer is favorable due to the larger electronegativity of the halogens and the

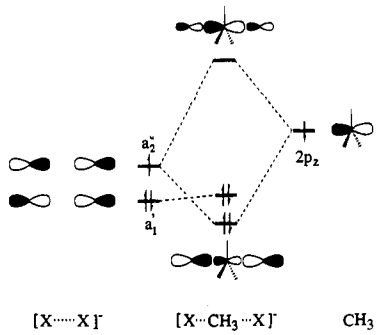

Figure 9. Orbital interaction diagram for the formation of the $X-CH_3-X$ bond in the transition state.

resulting charge separation helps further to reduce the electron–electron repulsion. We have also calculated the bonding overlap in $1a_2''$ of Figure 9 and found that it follows a trend opposite to $-\Delta E_{orbit}$. Thus, it is the polarization of the $[X\cdots CH_3\cdots X]^-$ bond, rather than the overlap involved, that determines its strength.[47] This conclusion is quite similar to that reached for the C–X bond in CH_3X.

The ETS analyses further revealed that the steric interaction between $[X\cdots X]^-$ and $\cdot CH_3$ is dominated by the Pauli repulsion term ΔE_{Pauli} which is due mainly to the repulsive interaction between the occupied a_1' symmetry fragment orbitals $a_1'([X\cdots X]^-)$ and $2s^2(C)$, Figure 9. The ΔE_{prep} contribution is mainly associated with the formation of $[X\cdots X]^-$ from X and X^-. The term ΔE_{prep} is stabilizing (negative) and follows as expected the same trend as the electronegativity of X.

IV. Concluding Remarks

We have carried out a comprehensive study on the potential energy surfaces of the title reactions. The study compares results from calculations based on density functional theory and ab initio methods and assesses the accuracy of different levels of theory within the DFT and ab initio categories. We have further explored and rationalized how periodic trends within the halogen family influence the potential energy surface of the title reactions. Our study was based on characterizing the crucial parts of the potential energy surfaces by optimizing geometries, calculating vibrational frequencies, and analyzing the carbon–halogen bonds for the reactants (products), complexes, and transition states. We have finally traced the intrinsic reaction path for the title reaction in the case of chlorine following two alternative routes. The main conclusions of this study can be summarized as follows:

(1) Ab initio calculations have demonstrated that electron correlation lowers the S_N2 barrier heights for all the halogens provided that use is made of extensive basis sets. Electron correlation will in addition enhance the complexation energy for the ion–dipole adduct $X^-\cdots CH_3X$. It was also demonstrated that the HF barriers are increased with the size of the basis set.

(2) Geometrical parameters and harmonic frequencies obtained by the DFT-based methods are in as good agreement with available experimental estimates as data obtained by the MP2 scheme. Similar conclusions have been drawn in previous studies[12a,b,29a] on other systems.

For calculations of the $X-CH_3$ bond dissociation energies, the nonlocal DFT scheme performs better than the MP2 and MP4 methods. This is true especially for the $F-CH_3$ bond, where the MP*n* methods underestimate the bond energy by about 10 kcal/mol whereas the NL-SCF and NL-P values deviate from the experimental date by less than 1 kcal/mol. The LDA scheme overestimates in all cases the $X-CH_3$ bonding energy by close to 30% whereas the HF method only accounts for 50% of the experimental dissociation energy. The nonlocal NL-SCF method and the MP*n* ($n = 2, 4$) schemes afford quite similar complexation energies for the ion–dipole adduct $X^-\cdots CH_3X$ for X = Cl, Br, and I. However, in the case of fluorine the MP*n* ($n = 2, 4$) binding energies are smaller than the NL-SCF estimate by 6 kcal/mol.

The barrier heights predicted by the ab initio and DFT methods turn out to be qualitatively different. The ab initio barriers are in general positive whereas the DFT barriers always are negative. It was found that the calculated barriers follow the general trend LDA $\ll$ NL-SCF $\ll$ MP4 < MP2 $\ll$ HF with respect to the different methods under investigation for all the halogen systems. The experimental barriers appear to lie between the NL-SCF and MP4 estimates.

(3) The influence of relativity on the geometries, frequencies, and relative energies of the closed shell reactants, ion–dipole complexes, and transition states was found to be negligible even for the heavier halogen systems of bromine and iodine. However, relativity was found to influence the $X-CH_3$ bond energies through the spin–orbital splitting in the open shell halogen atoms. Thus, the spin–orbital splitting correction to the $I-CH_3$ bond dissociation energy is as large as −7.2 kcal/mol.

(4) A detailed analysis has been carried out on the $X-CH_3$ and $X^-\cdots CH_3X$ bonds based on the extended transition state (ETS) scheme.[26] The trend in the $X-CH_3$ bond strengths follows the order F > Cl > Br > I, and this order is set by the electronegativity of the halogen through the amount of charge transferred from the CH_3 fragment to X rather than the bonding overlap which follows the reversed order. Thus, bond polarization rather than orbital overlap governs the strength of the $X-CH_3$ bond.

For the $X^-\cdots CH_3X$ complex, the electrostatic ion–dipole interaction contributes 15–25% of the interaction energy whereas the rest comes from X^- to CH_3X charge transfer. The amount of charge transfer increases with the electronegativity of the halogen and the complexation energy follows as a consequence the order F > Cl > Br > I.

The energy of the S_N2 transition state $[X\cdots CH_3\cdots X]^-$ relative to the reactants X^- and CH_3X, ΔE^C of Figure 1, is lowered as the polarization of the C–X bonds increases from iodine through fluorine. The overlaps in the three-center two-electron bonding orbital $1a_2''$ of Figure 9 follows the opposite pattern, and can thus not be responsible for the trend in ΔE^C as a function of X.

(5) Complete intrinsic reaction path (IRP) calculations carried out on the S_N2 reaction and the alternative halogen exchange process in the case of the chlorine system have elucidated the shape of the potential energy surface as well as the reaction mechanism.

Acknowledgment. This investigation was supported by the Natural Sciences and Engineering Research Council of Canada (NSERC). We gratefully acknowledge the donors of the Petroleum Research Fund, administered by the American Chemical Society (ACS-PRF No. 27023-AC3). We thank Dr. J. Li for useful discussions and Professor R. J. Boyd for valuable information.